

# Effect of thermal history on the superplastic expansion of argon-filled pores in titanium: Part I kinetics and microstructure

N.G.D. Murray<sup>1</sup>, D.C. Dunand<sup>\*</sup>

*Department of Materials Science and Engineering, Northwestern University, 2220 Campus Dr., Evanston, IL 60208, USA*

Received 15 October 2003; received in revised form 29 January 2004; accepted 29 January 2004

## Abstract

Titanium was foamed at high temperature by expanding pressurized argon bubbles which had been trapped in the metal during prior hot-isostatic pressing. During foaming, transformation superplasticity was induced in the matrix by thermal cycling around the  $\alpha/\beta$  allotropic temperature of titanium, thus accelerating pore growth and delaying cell wall fracture and pore opening to the surface, as compared to foaming performed exclusively under isothermal creep conditions in the  $\beta$ -Ti field. The relative importance of creep and superplastic deformation upon foaming rate, rate of porosity opening and maximum porosity was studied by changing the thermal cycling frequency and maximum temperature. Under superplastic conditions, porosity ceased to increase when reaching levels between 29% and 44%, principally because of the decrease of internal gas pressure due to pore expansion and, to a lesser extent, because of premature gas escape from the pores. Continued thermal cycling after the maximal porosity had been reached lead to pore coalescing and opening to the specimen surface by localized pore wall rupture, which resulted in large open pores with a jagged morphology.

© 2004 Acta Materialia Inc. Published by Elsevier Ltd. All rights reserved.

*Keywords:* Metals; Foams; Creep; Porosity; Superplasticity

## 1. Introduction

Unlike low-melting metals such as aluminum, magnesium or zinc, titanium and its alloys cannot be foamed in the liquid state because of their high melting temperature and extreme chemical reactivity, leading to contamination and embrittlement. Titanium foams are thus best produced in the solid-state, as first described by Kearns et al. [1–3] for Ti–6Al–4V and subsequently by others for Ti–6Al–4V [4–8] and unalloyed titanium [9]. In a first step, titanium or titanium alloy powders are densified by hot isostatic pressing within a sealed canister containing argon gas. The resulting compacted billet contains a small volume fraction (typically <1 vol%) of discreet, micron-sized pores filled with high-

pressure argon. In a second step, the billet is exposed to elevated temperatures at ambient pressure or vacuum, and the pressurized pores expand by creep of the surrounding metal. Kearns et al. [1–3] achieved porosities of up to ~40% in Ti–6Al–4V after exposure to very high temperatures (1240 °C) for long hold times (several days). The growth rate of the pores was controlled by the slow creep deformation of the metal, and was shown to increase by increasing the foaming temperature or the amount of argon gas entrapped during densification. In previous publications [9–11], we demonstrated that deformation of the titanium matrix surrounding the pressurized argon pores could be enhanced by using transformation superplasticity, therefore significantly increasing both the foaming (pore growth) rates and the maximum achievable porosity. Transformation superplasticity is exhibited by polymorphic materials, such as pure titanium [12,13], Ti–6Al–4V [14–16] and many other polymorphic metals and alloys [12,17]). Deformation occurs when internal strains, which are created

<sup>\*</sup> Corresponding author. Tel.: +1-847-491-5370; fax: +1-847-467-6573.

E-mail address: [dunand@northwestern.edu](mailto:dunand@northwestern.edu) (D.C. Dunand).

<sup>1</sup> Formerly known as N.G. Davis.

by the mismatch in density between the two allotropic phases coexisting during a phase transformation, are biased by an externally applied stress. By repeatedly cycling through the phase transformation during uniaxial tension of fully dense materials, the strain increments developed in the direction of the biasing stress during the phase transformation can be accumulated to well in excess of 100% without fracture or cavitation. Using the argon pressure within the pores of the densified billets as the biasing stress, we recently demonstrated that foaming titanium under transformation-superplasticity-dominated conditions by thermal cycling about the allotropic temperature leads to faster foaming rates and higher terminal porosities than under isothermal conditions, where the deformation is dominated by creep [9–11].

In the present article, we systematically investigate how thermal cycling temperatures and rates affect pore growth kinetics and total achievable porosity during the solid-state foaming of titanium. Additionally, we compare these data with isothermal creep data. In a companion article [18], we present analytical and numerical models to explain our results.

## 2. Experimental procedures

Spherical, commercially pure titanium (CP-Ti) powders (from Starmet, Concord, MA) were sieved to  $-200/+230$  mesh (62–88  $\mu\text{m}$  range, with an average of 75  $\mu\text{m}$ ). The powders were packed in a mild-steel can, backfilled with 3.3 atm argon and densified at 890  $^{\circ}\text{C}$  for 2 h under 100 MPa argon gas at Connaway Technologies and Isostatic Forging (Hilliard, OH). After consolidation, the billets contained very small pores with a volume fraction of 0.15%, as illustrated in Fig. 1.

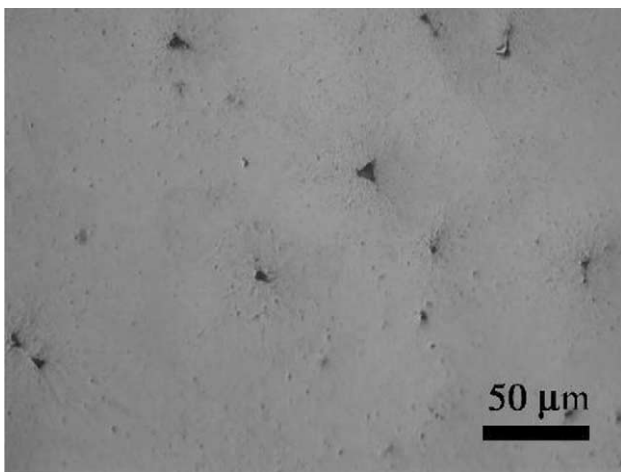


Fig. 1. Optical micrograph of as-densified CP-Ti: irregularly shaped Ar-filled pores at interstices of prior (non-visible) powder particles.

Five thermal cycling experiments were performed on cubic specimens with 9 mm edges produced by electro-discharge machining, varying cycle frequency and maximum temperature in the thermal cycle. All thermal cycles spanned the allotropic temperature range of CP-Ti (nominally 882  $^{\circ}\text{C}$ , but expected to be higher and wider because of oxygen content [19,20]). Triangular thermal cycles were used, with the following upper/lower temperatures and period: 830–930  $^{\circ}\text{C}/13$  min, 830–980  $^{\circ}\text{C}/2, 4,$  and 20 min, and 830–1050  $^{\circ}\text{C}/30$  min. Isothermal experiments were performed at 980  $^{\circ}\text{C}$  (one of the upper cycle temperatures) and at 903 and 955  $^{\circ}\text{C}$ , corresponding to the effective temperature for the 830–980 and 830–1050  $^{\circ}\text{C}$  cycles, respectively. The effective temperature is defined as the temperature at which the isothermal creep rate is the same as the time-averaged creep rate during thermal cycling in the absence of transformation-superplasticity [13,14], and was calculated using creep activation energies given in [21] for  $\alpha$ -Ti and  $\beta$ -Ti. Thus, by comparing foaming kinetics under thermal cycling conditions with those at the effective temperature, the effect of superplasticity on foaming is directly revealed. The effective temperature for the 830–930  $^{\circ}\text{C}$  cycles is undefined due to the discontinuous nature of the diffusion coefficients for  $\alpha$ -Ti and  $\beta$ -Ti.

The three thermal cycling experiments with longer periods and the three isothermal experiments were performed under flowing argon in an Orton 1600D dilatometer (Westerville, OH) with a heating/cooling rate of 15  $^{\circ}\text{C}/\text{min}$  on specimens coated with Deltaglaze 153<sup>TM</sup>, a borosilicate glass from Acheson Colloids (Port Huron, MI), to protect from contamination by residual oxygen and nitrogen. The cycling experiments with 2 and 4 min periods were performed in a custom-built radiative furnace [22], also under a flowing argon atmosphere, with a 300  $^{\circ}\text{C}$  burn-off for 1 h and a heating rate from 300 to 830  $^{\circ}\text{C}$  of 75  $^{\circ}\text{C}/\text{min}$ . Foaming was frequently interrupted by excursions to room temperature for density determination by the Archimedes method in distilled water. A thin layer of vacuum grease was applied to the specimen surface to prevent water infiltration into the open porosity, thus yielding a direct measurement of specimen total porosity. Density was also measured by helium pycnometry (using an Accupyc 1330 from Micromeritics, Norcross, GA) on unsealed specimens, allowing for measurement of closed porosity. Open porosity was calculated as the difference between total and closed porosity.

After foaming completion, specimens were cut in half along one of the cube face diagonals with a low-speed diamond saw, mounted in acrylic resin, and polished to 0.05  $\mu\text{m}$  alumina. To retain the original pore shape during polishing, pores were vacuum-infiltrated with the same acrylic resin used to mount the specimens at regular intervals during polishing.

### 3. Results

#### 3.1. Effect of cycling on foaming rate

Fig. 2 shows specimen porosity as a function of time for the first 60 h of foaming with 830–980 °C/4 min cycles and for isothermal foaming at 903 and 980 °C. After 60 h, the thermally cycled specimen yields much higher total porosity  $p$  ( $p = 44\%$ ) than isothermal foaming at either the effective temperature of 903 °C ( $p = 12\%$ ), or the maximum cycle temperature of 980 °C ( $p = 18\%$ ). Both isothermal foaming curves in Fig. 2 continue to show a shallow increase in porosity with time after 60 h, while the curve for the thermally cycled specimen reached a maximum in total porosity at  $p = 44\%$  after ca. 35 h.

#### 3.2. Effect of effective temperature on foaming rate

The effect of varying the effective temperature on foaming rate and total porosity is illustrated in Fig. 3, which shows the time dependence of the specimen total porosity for thermal cycles with maximum temperatures of 930, 980 and 1050 °C together with isothermal foaming curves at 903, 955 and 980 °C. For thermal cycles, the highest and lowest porosities ( $p = 35\%$  and  $29\%$ , respectively) were achieved for maximum temperatures of 980 and 1050 °C, respectively. For cycles with the lowest maximum temperature (930 °C), the maximum porosity was  $p = 34\%$ , but the time to reach that porosity ( $\sim 90$  h) was ca. double that observed for the other thermal cycles. The foaming rates for isothermal

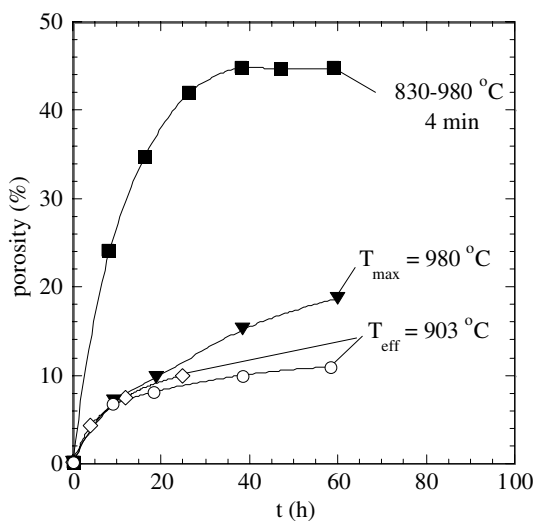


Fig. 2. Total porosity as a function of time during thermal cycling (830–980 °C) and isothermal foaming at 903 or 980 °C. The circles and the triangles correspond to heating rates of 15 °C/min (performed in the dilatometer) to the isothermal foaming temperature, while the diamonds and squares had a 75 °C/min heating rate.

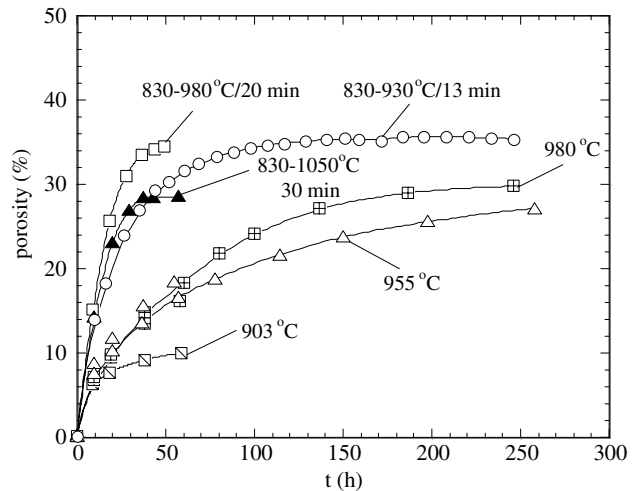


Fig. 3. Total porosity as a function of time for three thermal cycles (830–930 °C/13 min, 830–980 °C/20 min and 830–1050 °C/30 min) compared to isothermal anneals at the effective temperatures of the thermal cycles (903 and 955 °C) and isothermal anneal at the upper temperature of the 830–980 °C/20 min cycle.

foaming at 980 and 955 °C are similar up to about  $p = 15\%$ , after which isothermal foaming at 980 °C becomes faster; isothermal foaming at 903 °C is slowest. In all cases, thermal cycling resulted in faster foaming rates and higher porosities than foaming at the corresponding effective temperature or the maximum temperature of a particular thermal cycle. For instance, at 903 °C (which is the effective temperature of the 830–980 °C cycle), a small value of  $p = 11\%$  was achieved after foaming for 60 h. Even at 980 °C, only  $p = 15\%$  is achieved after 40 h as compared to  $p = 35\%$  for the 830–980 °C cycles. Extremely long annealing times are required ( $\sim 8$  days) to achieve a relatively high value of  $p = 30\%$ , which is reached in ca. 24 h using 830–980 °C cycles. Similar trends are visible when comparing the curve for 830–1050 °C thermal cycles with the curve at the effective temperature of 955 °C.

#### 3.3. Effect of cycle frequency on foaming rate

The time-dependence of porosity is shown in Fig. 4 for the 830–980 °C thermal cycles with 2, 4 and 20 min cycle periods. In general, the shorter the cycle period is, the faster the initial foaming rate. However, the fastest cycle (2 min) yields a lower maximum porosity than the 4 min thermal cycle, i.e.,  $p = 39\%$  vs.  $44\%$ . Conversely, the slowest thermal cycle (20 min) yields the lowest maximum porosity ( $p = 35\%$ ).

Fig. 5 shows the porosity data from Figs. 3 and 4 plotted as a function of cycle number rather than time. The 830–1050 °C/30 min cycle induces the largest increase in porosity per thermal cycle during the initial stages of foaming, until reaching a plateau at  $p = 29\%$  after 75 cycles. Beyond that point, the 830–980 °C/20

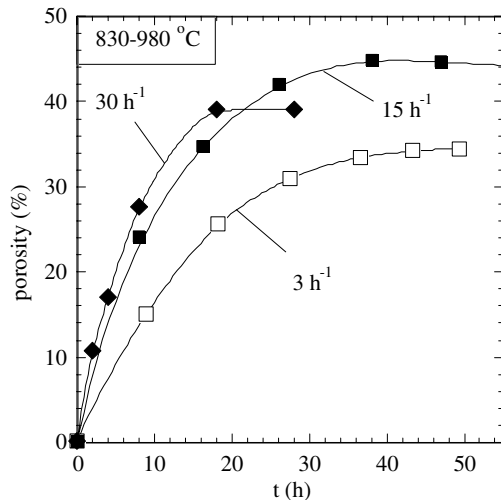


Fig. 4. Total porosity as a function of time for 830–980 °C thermal cycles with various period: 2 min (30 h<sup>-1</sup>); 4 min (15 h<sup>-1</sup>); and 20 min (3 h<sup>-1</sup>) cycles.

min cycle, which begins with a slightly lower porosity increase per cycle, continues to increase in porosity, until reaching a plateau at  $p = 34\%$ . Comparing the three curves for the 830–980 °C cycles (with 2, 4 and 20 min cycles), it is apparent that the shorter the cycle is, the lower the porosity increase per cycle. Finally, Fig. 5 shows that the 830–930 °C/13 min and the 830–980 °C/4 min curves are almost overlapping. This illustrates that a lower maximum temperature can be compensated with a longer cycle duration.

### 3.4. Evolution of open porosity

Representative curves for total, closed and open porosity are shown in Figs. 6(a) and (b) as a function of

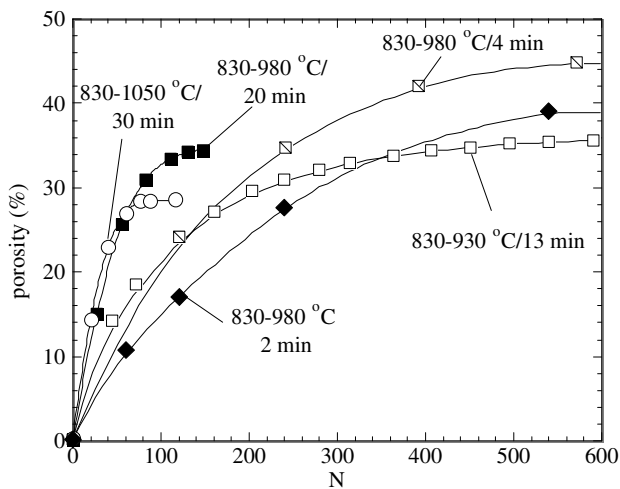


Fig. 5. Evolution of porosity with thermal cycle number (up to 600 cycles) for all studied thermal cycling conditions.

foaming time for two thermal cycles. For all five cycling experiments, the specimen porosity remains completely closed during the initial stages of foaming. Onset for the opening of porosity is affected by the type of thermal cycle: 830–980 °C/4 min thermal cycles (Fig. 6(a)) achieve a higher total porosity than the 830–980 °C/20 min cycles (Fig. 6(b)) before an appreciable portion of the porosity begins to open to the specimen surface:  $p = 41\%$  vs.  $p = 26\%$ , respectively. In addition, the 4 min cycles rapidly open existing porosity to the specimen surface (Fig. 6(a)), even after there is no further increase in total porosity with continued thermal cycling. However, for the 20 min cycles (Fig. 6(b)), as the porosity begins to open, there is still a significant increase in total porosity until after about 40 h, when the total, open and closed porosity remain constant.

Total, closed, and open porosity behavior for the 830–980 °C/2 min and 830–930 °C/13 min cycles are similar to that for the 830–980 °C/4 min thermal cycles (Fig. 6(a)). However, porosity (total, closed and open) evolution for the latter cycle is much slower. Also, the foaming curves for the 830–1050 °C/30 min cycle thermal cycles are similar to those for the 830–980 °C/20 min cycles (Fig. 6(b)). However, pores begin to appreciably open to the specimen surface at lower amount of total porosity ( $p = 15\%$  vs.  $p = 26\%$ ) and at earlier foaming times ( $\sim 10$  vs.  $\sim 20$  h). With increasing the upper temperature from 930 to 980 and to 1050 °C, the time needed for opening the porosity decreases, as does the total porosity at which this event occurs.

Finally, Fig. 6(c) shows the case of isothermal foaming at 980 °C: the relative open porosity ratio  $F$  (ratio of open porosity to total porosity) is  $F < 0.10$  after 60 h of foaming and increases to only  $F = 0.38$  after a very long heat treatments of 250 h. Thus, the open porosity evolution is much more gradual for isothermal foaming at 980 °C than for foaming under thermal cycling conditions, which is correlated with the slower foaming rates during isothermal creep foaming. This temperature, the highest studied here, is the only one leading to appreciable open porosity during isothermal foaming.

### 3.5. Microstructure

#### 3.5.1. Isothermal foaming

Figs. 7(a)–(c) show representative pore morphologies resulting from isothermal foaming at 903 °C for 60 h, 955 °C for 250 h and 980 °C for 250 h. As shown in Fig. 3, pore growth for each of these time/temperature combinations has virtually stopped. Thus, these three microstructures can be compared to each other, despite the great disparity in foaming time. At low porosity ( $p = 11\%$ ), the pores remain discrete, with few coalesced pores and only a few pores exceeding a size of 75  $\mu\text{m}$ , as shown in Fig. 7(a) for foaming at 903 °C. However, for

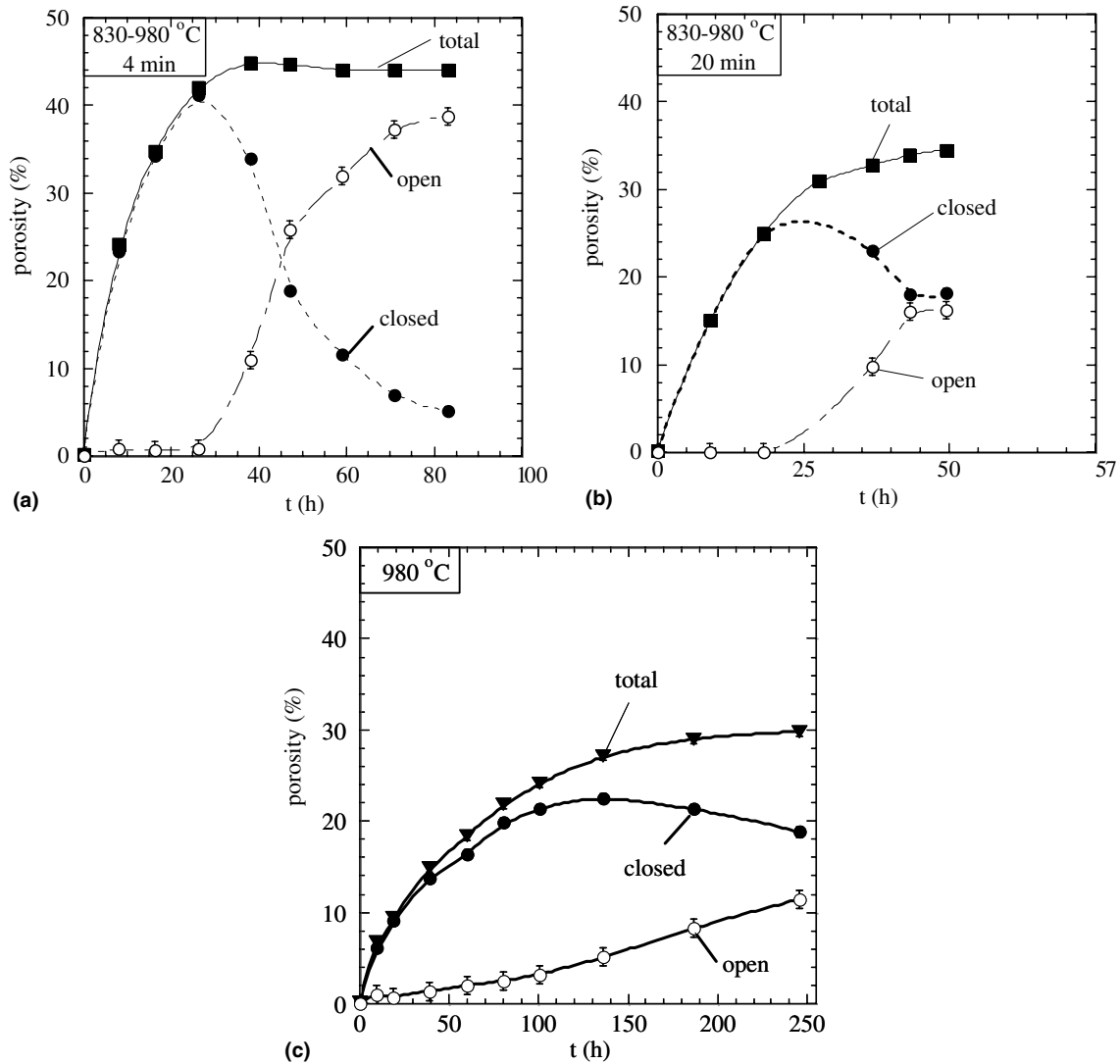


Fig. 6. Total, closed and open porosity as a function of time for various thermal cycles: (a) 830–980 °C/4 min; (b) 830–980 °C/20 min; (c) isothermal foaming at 980 °C.

foaming at 955 and 980 °C with  $p = 27\%$  and  $30\%$ , respectively (Figs. 7(b) and (c)), specimens show many more coalesced pores with dimensions exceeding 75  $\mu\text{m}$ . In particular, many more coalesced pores are visible for isothermal foaming at 980 °C (Fig. 7(c)) as compared to 955 °C (Fig. 7(b)), despite only a slightly higher total porosity. This difference is also reflected by the much higher open porosity ratio ( $F = 0.38$  and  $0.04$ , respectively). Finally, many of the pores in the isothermally foamed specimens are faceted (arrow in Fig. 7(a)).

Fewer very large pores are visible after isothermal foaming at 955 °C than after isothermal foaming at 980 °C, further supporting the open porosity measurements that pore coalescence has taken place to a much greater extent at 980 °C. In fact, for that specimen, several regions were observed where multiple pores have joined, leaving round (presumably spherical in three-dimensions) powder particles of about 75  $\mu\text{m}$  in diameter

protruding within elongated pores (arrows in Fig. 7(c)), suggesting coalescence of pores surrounding several individual powder particles.

### 3.5.2. Thermal cycling

Figs. 8(a)–(d) show representative microstructures resulting from foaming with 830–980 °C/4 min cycles ( $p = 44\%$ ,  $F = 0.88$ ), 830–980 °C/20 min cycles ( $p = 35\%$ ,  $F = 0.47$ ), 830–930 °C/13 min cycles ( $p = 36\%$ ,  $F = 0.82$ ), and 830–1050 °C/30 min cycles ( $p = 29\%$ ,  $F = 0.44$ ), respectively. Specimens with a high relative open porosity ratio,  $F$ , have a larger pore size than those with more closed porosity, as seen by comparing Figs. 8(b) and (c), where both have similar total porosity ( $p = 35\%$  and  $36\%$ , respectively), but open porosity ratio which varies by a factor two ( $F = 0.47$  and  $0.82$ , respectively). Pore sizes of ca. 200–800  $\mu\text{m}$  can be observed in the specimen with more open porosity (Figs. 8(a) and (c))

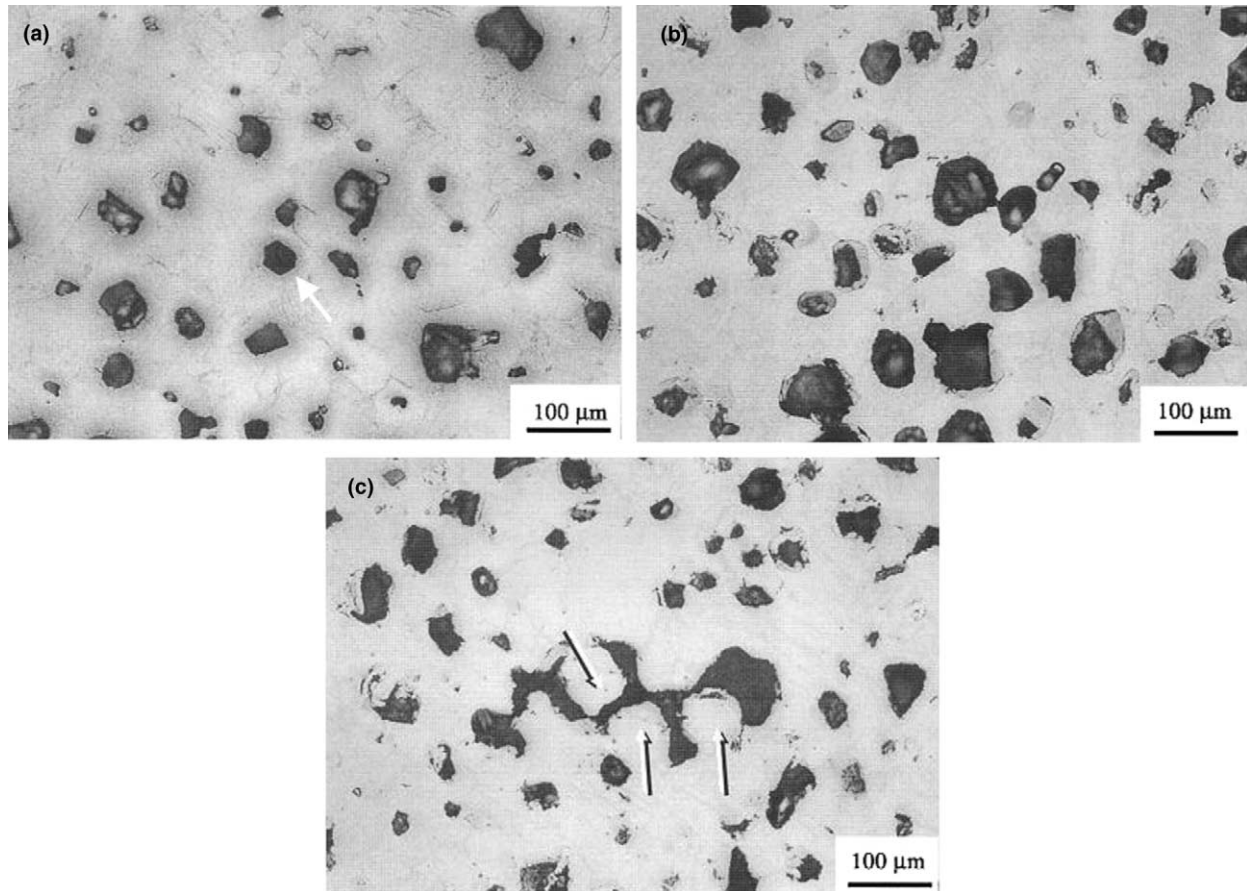


Fig. 7. Optical micrographs showing the pore morphology for isothermal foaming: (a) 903 °C ( $p = 11\%$ ,  $F = 0$ ), (b) 955 °C ( $p = 27\%$ ,  $F = 0$ ) and (c) 980 °C ( $p = 30\%$ ,  $F = 0.38$ ); round protrusions (arrows) correspond to powder particles.

while pores rarely exceed 150  $\mu\text{m}$  for those with less open porosity (Figs. 8(b) and (d)). In all cases, thin titanium walls separating pores (some as small as 20  $\mu\text{m}$ ) are present after thermal cycling (arrows in Fig. 8), but are not observed after isothermal foaming.

## 4. Discussion

### 4.1. Isothermal foaming

Fig. 3 shows that solid-state foaming by isothermal creep expansion of high-pressure argon-filled pores, even at relatively high homologous temperatures, results in slow foaming rates and low porosities (except after many days). This is in qualitative agreement with previous results for solid-state foaming of Ti–6Al–4V [1–3,5–8] (those studies used different initial gas pressure and powder size) and with our previous studies for CP-Ti [9] using un-sieved powders (100 mesh, average size 130  $\mu\text{m}$ ).

Foaming rates increase only slightly from 955 to 980 °C (Fig. 3), as expected, since the steady-state  $\beta$ -Ti creep rate increases only by a factor 1.4 between these tem-

peratures [21]. The significantly lower isothermal foaming rate at 903 °C can be explained by the hypothesis that, due to oxygen contamination, the present CP-Ti foams are in the  $\alpha$ -Ti phase field at 903 °C, or in the  $\alpha + \beta$ -Ti, two-phase field; at the same (hypothetical) temperature,  $\alpha$ -Ti creeps at a rate that is about 10 times slower than  $\beta$ -Ti.

In terms of maximal porosity, isothermal foaming can, in some cases, achieve the same values as thermal cycling, albeit after much longer time (250 vs. 35 h. in Fig. 3). The highest porosity achieved isothermally ( $f = 30\%$  at 980 °C, Fig. 3) however falls well short of the maximum porosity achievable under thermal cycling ( $f = 44\%$ , 830–980 °C/4 min, Fig. 6(a)).

The maximum porosity achievable during foaming is controlled by the decrease in pore pressure associated with the increase in pore volume, resulting in pore growth that becomes too slow to measure. However, premature foaming cessation can occur if pores connect with the specimen surface, so that the pressurized argon escapes to the ambient atmosphere and the driving force for further pore expansion disappears. Superplastic foaming improves the maximum porosity achievable over creep foaming by acting on both mechanisms.

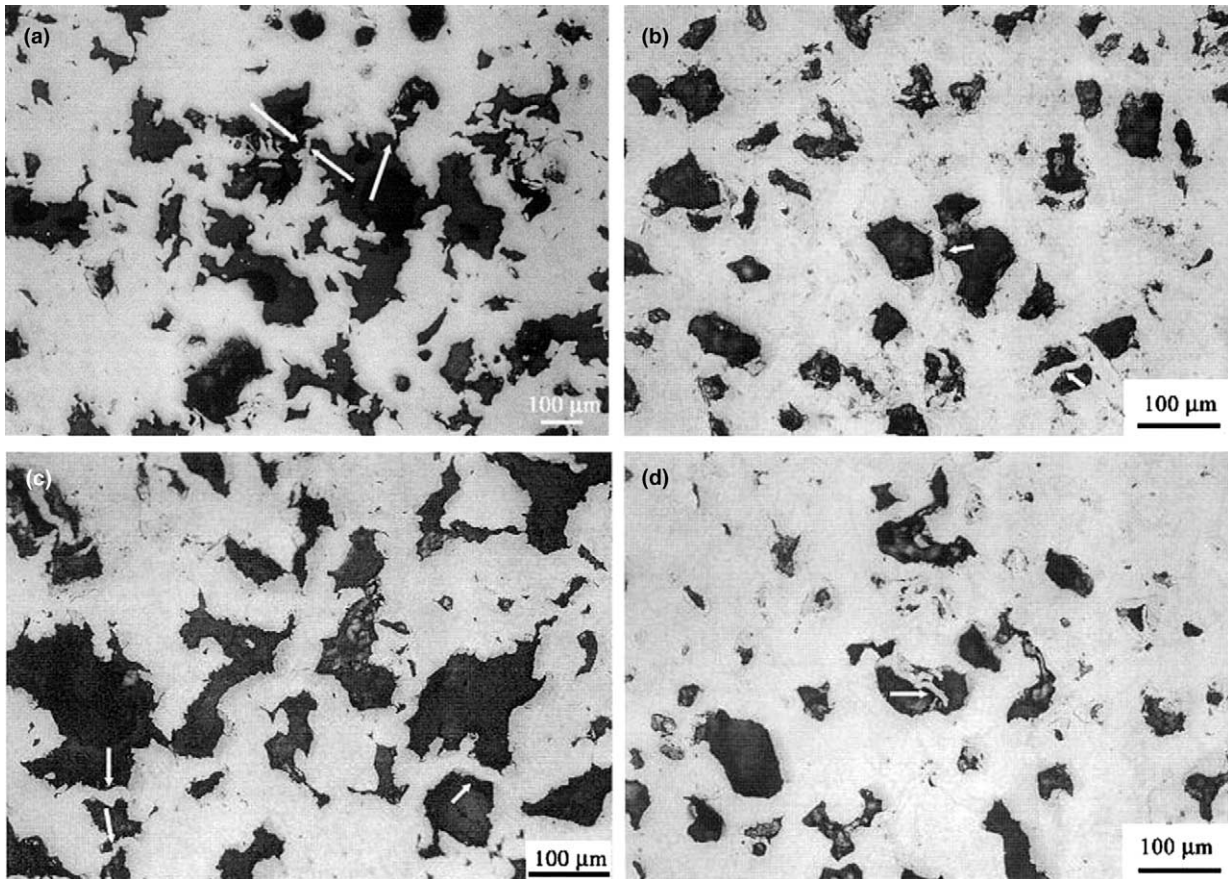


Fig. 8. Optical micrographs showing the pore morphology for various thermal cycles: (a) 830–980 °C/4 min cycle ( $p = 44\%$ ,  $F = 0.88$ ), (b) 830–980 °C/20 min cycle ( $p = 35\%$ ,  $F = 0.47$ ) (c) 830–930 °C/13 min cycle ( $p = 36\%$ ,  $F = 0.82$ ), and (d) 830–1050 °C/30 min ( $p = 29\%$ ,  $F = 0.44$ ). Arrows indicate thin walls, some of which are ruptured.

First, superplasticity allows for significant deformation at stresses lower than during creep, so isolated pores will expand to larger terminal size under superplastic conditions. Second, since pore coalescence and opening to the specimen surface is the result of tensile fracture in the walls separating the pores, and since much larger tensile fracture strains are achievable under superplastic conditions, pores can grow to larger sizes prior to pore wall fracture and the escape of gas during superplastic foaming, as compared to creep foaming.

#### 4.2. Foaming by thermal cycling

Neglecting any small variation in argon pressure due to thermal cycling (the pore pressure at a maximum temperature of 1050 °C is 20% higher than at 830 °C), the enhancement due to transformation superplasticity during foaming can be directly visualized during foaming by thermal cycling to isothermal foaming at the corresponding effective temperature. Figs. 2 and 3 show that the overall foaming rate is significantly higher under thermally cycled, superplastic conditions for any of the thermal cycles presented here (830–980 °C/4 min, 830–980 °C/20 min, or 830–1050

°C/30 min) as compared to foaming under creep conditions at the effective temperatures (903 and 955 °C, respectively). As mentioned earlier, an effective temperature for the 830–930 °C/13 min cycle is non-existent. However, when comparing this cycle to isothermal foaming at 903, 955 or even 980 °C, it is observed from Fig. 3 that this thermal cycle under superplastic conditions still enhances foaming over isothermal foaming. This is consistent with our previous study for preforms with un-sieved CP-Ti powders [9], and in agreement with the observation that deformation of bulk CP-Ti and Ti–6Al–4V samples subjected to uniaxial [13] and multiaxial [14,23] stress under transformation superplastic conditions is faster than under isothermal creep conditions.

For the cycles having the same peak temperatures of 980 °C (Fig. 4), the initial rate of foaming decreases with increasing thermal cycling duration: for the 2, 4 and 20 min cycles, average initial foaming rate of  $10 \times 10^{-6}$ ,  $8 \times 10^{-6}$  and  $5 \times 10^{-6} \text{ s}^{-1}$ , respectively, are found (approximated by taking the total porosity after 8–9 h and dividing by the foaming time). This illustrates that, during a thermal cycle, the dominant mechanism for pore growth is superplasticity during the phase trans-

formations, rather than creep above the transformation temperature. Thus, assuming full transformation of the specimen, the more frequent the excursions through the phase transformation (i.e., the faster the cycles), the higher the average foaming rate.

Similarly, the 830–1050 °C/30 min thermal cycle has a slower foaming rate when compared to any of the faster 830–980 °C cycles (2, 4 or 20 min). However, the 830–1050 °C/30 min cycle (Fig. 3) yields about the same foaming rate as for the 830–930 °C/13 min cycle, despite a cycle duration longer by a factor 2.3 (and thus less than half the contribution of superplastic foaming per unit time). This illustrates that transformation superplasticity contributions (higher in the 830–930 °C experiments with fast cycling) and creep contribution (higher in the 830–1050 °C experiments with high maximum temperature) can both contribute significantly to the foaming rates.

The effect of creep is further visible in Fig. 5, where porosity is displayed as a function of the number of thermal cycle, which normalizes the superplastic contribution for all experiments. Differences are thus solely due to the creep contribution, which is expected to increase with increasing peak temperature and with increasing cycle length. Indeed, the highest initial foaming rate in Fig. 5 (before onset of the plateau) corresponds to the 830–1050 °C/30 min cycle, which has both the highest peak temperature and longest cycle length. The lowest initial foaming rate corresponds to the 830–980 °C/2 min cycles, which exhibit the shortest cycle length. We note that creep is expected to contribute significantly to foaming only for the time spent in the  $\beta$ -Ti field, as  $\alpha$ -Ti creeps much more slowly than  $\beta$ -Ti [21].

As discussed in the previous section, maximum achievable porosity is expected to increase with increasing superplasticity contribution and decreasing creep contribution, because of both the lower strength and higher ductility exhibited by titanium under superplastic conditions. In Fig. 3, where the upper cycling temperature is varied, it is apparent that the cycles with the most creep and least superplasticity (830–1050 °C/30 min) indeed result in the lowest maximum porosity ( $p = 29\%$  vs.  $p = 35\text{--}36\%$ ). Similarly, in Fig. 4 where only the cycle frequency is varied, the longest cycles (830–980 °C/20 min) with the most creep also induce the lowest maximum porosity ( $p = 35\%$  vs.  $p = 39\text{--}44\%$ ).

Unexpectedly, the 4-min thermal cycles achieve a higher porosity level ( $p = 44\%$ ) than the 2 min cycles ( $p = 39\%$ ), despite a smaller superplastic contribution (Fig. 4). This may be explained by the fact that the former foam exhibited more contamination from the atmosphere, as evidenced by its oxygen chemical analysis and mass-grain rate. This oxygen contamination likely increased the  $\alpha/\beta$  transus temperature, thus reducing the amount of time spent creeping in  $\beta$ -Ti phase.

### 4.3. Closed and open porosity

The total, closed and open porosity values presented in Figs. 6(a)–(c) for thermal cycling and isothermal foaming indicate that almost all pores in all specimens remain closed during the early stages of foaming. The thermal cycle with the highest creep contribution (830–1050 °C/30 min) exhibits the lowest amount of total porosity ( $p = 18\%$ ) and shortest amount of time ( $\sim 15$  h) for the onset of porosity opening to the specimen surface. Once coalesced pores connect to the specimen surface, the total porosity for the 830–1050 °C/30 min as well as the 830–980 °C/20 min cycles (Fig. 6(b)) continues to increase with thermal cycling. This indicates that porosity opens prematurely to the surface, well before the pressure in the pores is too low for further pore expansion. Both of these cycles have the same relative open porosity ratio,  $F \sim 0.5$ , at pore growth cessation.

On the other hand, higher frequency cycles where transformation superplasticity is more dominant (illustrated in Fig. 6(a)) result in negligible open porosity almost up to the point where the maximum total porosity is attained, indicating that no gas escapes until the pore pressure is too low for further foaming, i.e., until the maximum achievable porosity has been reached. With further thermal cycling, open porosity continues to increase in a gradual manner without a corresponding increase in total porosity, as pores increasingly interlink with each other and the specimen surface. This is likely due to the fracture of very thin pore walls, which occurs by localized deformation, at stresses too low for global sample growth. Except for the 830–930 °C/13 min cycles, the time from the onset of porosity opening ( $F = 0$ ) to the point where half the porosity is open ( $F = 0.5$ ) is near constant at ca. 20 h., independently of the number of thermal cycles. This indicates that initial pore opening is dominated by the total amount of time spent in the  $\beta$ -Ti field where creep strain is accumulated in the walls separating pores, not by the total amount of superplastic strain in the walls. This is expected, as strain accumulated under creep conditions leads to fracture by rapid cavitation and necking (and thus pore wall rupture), unlike for superplastic deformation. Finally, the observation that the 830–930 °C/13 min cycles necessitate triple the amount of time (ca. 60 h) for  $F$  to increase from 0 to 0.5 can be explained by the fact that the creep contribution to wall deformation is the smallest for these cycles, due to the very low upper temperature. In summary, pore growth and pore coalescence are affected differently by the two deformation mechanisms: creep leads to slow pore growth and rapid pore coalescence, while transformation superplasticity has the opposite effect.

All isothermally foamed specimens remain almost entirely closed after ca. 50 h of foaming, beyond which

the 903 °C anneal was terminated. For isothermal foaming at 955 °C, porosity remains almost entirely closed even after 250 h ( $p = 27\%$ ) with a relative open porosity ratio,  $F \leq 0.10$ . For these two cases, the decrease in foaming rate is thus due primarily to the reduction in pore pressure with pore growth, not from loss of gas due to porosity opening to the specimen surface. However, as shown in Fig. 6(c), the specimen annealed at the highest temperature of 980 °C exhibits pores opening to the surface after reaching about  $p = 18\%$ ; this porosity value is similar to that for the 830–1050 °C/30 min thermal cycles, but is reached after a much longer time, because of the slow rate of foaming under isothermal creep conditions. Similarly, the rate at which porosity opens is much slower for the case of isothermal foaming (Fig. 6(c)), as compared to during thermal cycling. Thus, for isothermal foaming at 980 °C, a combination of the reduction in pore pressure due to pore growth, and removal of the driving force due to pore opening is the cause of the decrease in foaming rate observed with time.

#### 4.4. Pore morphology

Most of the pores resulting from isothermal foaming remain primarily equiaxed and are more rounded than in the as-densified state, where the pores exhibited sharp cusps, reflecting the original inter-powder spacing (Fig. 1). However, most pores are faceted, as illustrated in Fig. 7(a) (arrow) where a pore with an almost perfectly hexagonal cross-section is shown for isothermal foaming at 903 °C for 60 h. Similarly faceted pores were found for all isothermal foaming temperatures studied. During the first studies of isothermal foaming of Ti–6Al–4V in the  $\beta$ -phase, Kearns et al. [1,2] also found faceted pores with square cross-sections, which they attributed to low energy  $\{100\}$  planes of the Ti–6Al–4V  $\beta$ -phase matrix. This faceting, which occurs in our specimens in the  $\beta$ -Ti phase when growth of the pressurized pores is negligible, is similar to thermal etching on surfaces: gradients in surface energy promote surface diffusion, such that crystallographic planes with lower energy grow at the expense of higher energy planes. The equilibrium shape of such pores should be described by the Wulff plot for CP-Ti in an argon atmosphere, but will change with slight variation in composition [24–28].

With the opening of porosity by pore coalescence during thermal cycling, the pore morphology changes drastically. Foams with the same amount of total porosity, but with less open porosity, exhibit pores that are smaller and more equiaxed than those having more open porosity (e.g., comparing Figs. 8(b) and (c)). Additionally, as the amount of open porosity increases, the jaggedness of the pores increases. Both these effects are likely due to pore linkage. As pores coalesce by the rupture of thin walls between pores (as shown by the

arrows in Fig. 8) created by the large strains possible by thermal cycling-induced transformation superplasticity, remnants of the thin pore wall become protrusions into the pores, increasing their jaggedness. The size of these protrusions (typically 50  $\mu\text{m}$ ) is too large for diffusion to shrink them markedly at the times and temperatures used for foaming.

## 5. Conclusions

Solid-state foaming was performed under various processing conditions on CP-Ti (consolidated from 75  $\mu\text{m}$  powder) with 0.14% initial porosity of high-pressure argon-filled pores, leading to the following conclusions:

- Under isothermal conditions, foaming rates are lowest for at 903 °C, and higher at 955 and 980 °C, for which total porosities  $p = 28\text{--}30\%$  are reached after 250 h.
- Thermal cycling about the allotropic temperature, which activates transformation superplasticity in titanium, leads to accelerated foaming kinetics and increased maximum attainable porosity and pore size. This is because superplastic titanium exhibits reduced strength (opposing less resistance to gas expansion) and higher ductility (delaying fracture of the walls separating pores).
- For the same temperature range, faster thermal cycles lead to higher foaming rates and terminal porosity, because of a higher superplastic contribution and lower creep contribution to deformation in the cycle. Foaming stops primarily because of a decrease in pore pressure (from pore volume increase) but also from a loss of driving force (from gas escaping as porosity opens to the specimen surface).
- With increasing peak temperature and cycle duration, the creep contribution increases and so the porosity gain per cycle increases, but the total terminal porosity decreases. In addition, pores begin to open to the specimen surface at lower overall porosities and shorter times when the creep contribution increases.
- Just after reaching a plateau in porosity, most of the porosity in the thermally cycled foams remains closed (although some internal coalescence by pore wall rupture has occurred). With further thermal cycling, pores open to the specimen surface without increase in total porosity; extensive internal pores coalescence by pore wall rupture leads to a jagged pore morphology and long internal channels.

## Acknowledgements

This research was supported by US National Science Foundation through Grant DMR-0108342/001. NGDM also thanks the US Department of Defense for

a NDSEG Fellowship, the Zonta Foundation for the Amelia Earhart Fellowship, and the American Association of University Women for a Selected Professions Dissertation Year Fellowship.

## References

- [1] Kearns MW, Blenkinsop PA, Barber AC, Farthing TW. *Met Mater* 1987;3(2):85.
- [2] Kearns MW. Formation of porous bodies. IMI Titanium Limited, US Patent, 4659545; 1987.
- [3] Kearns MW, Blenkinsop PA, Barber AC, Farthing TW. *Int J Powder Metall* 1988;24(1):59.
- [4] Martin RL, Lederich RJ. *Metal Powder Rep* 1992;30–5.
- [5] Queheillalt DT, Choi BW, Schwartz DS, Wadley HNG. *Metall Mater Trans A* 2000;31(1):261.
- [6] Elzey DM, Wadley HNG. *Acta Mater* 2001;49(5):849.
- [7] Queheillalt DT, Gable KA, Wadley HNG. *Scr Mater* 2001; 44(3):409.
- [8] Vancheeswaran R, Queheillalt DT, Elzey DM, Wadley HNG. *Metall Mater Trans* 2001;32:1813.
- [9] Davis NG, Teisen J, Schuh C, Dunand DC. *J Mater Res* 2001;16:1508.
- [10] Murray NGD, Dunand DC. *Comp Sci Technol* 2003;63:2311.
- [11] Murray NGD, Schuh CA, Dunand DC. *Scr Mater* 2003;49:879.
- [12] Greenwood GW, Johnson RH. *Proc Roy Soc Lond A* 1965;283:403.
- [13] Dunand DC, Bedell CM. *Acta Mater* 1996;44(3):1063.
- [14] Dunand DC, Myojin S. *Mater Sci Eng A* 1997;230:25.
- [15] Schuh C, Dunand DC. *Acta Mater* 2001;49(2):199.
- [16] Schuh C, Dunand DC. *J Mater Res* 2001;16(3):865.
- [17] Nieh TG, Wadsworth J, Sherby OD. *Superplasticity in metals and ceramics*. Cambridge, UK: Cambridge University Press; 1997.
- [18] Murray NGD, Dunand DC. Effect of thermal history on the superplastic expansion of argon-filled pores in titanium: Part II modeling of kinetics. *Acta Mater* 2004, doi:10.1016/j.actamat. 2004.01.019.
- [19] Elmer JW, Wong J, Ressler T. *Metall Mater Trans A* 1998;29: 2761.
- [20] Szkliniarz W, Smolka G. *J Mater Proc Tech* 1995;53:413.
- [21] Frost HJ, Ashby MF. *Deformation-mechanism maps: the plasticity and creep of metals and ceramics*. Oxford: Pergamon Press; 1982. p. 44.
- [22] Zwigl P, Dunand DC. *Metall Mater Trans A* 1998;29:2571.
- [23] Frary M, Schuh C, Dunand DC. *Metall Mater Trans A* 2002;33:1669.
- [24] Bennett WD. *J Met* 1955;7:322.
- [25] Evans P. *Acta Metall* 1957;5:342.
- [26] Moore AJW. Thermal faceting. In: Robertson WD, Gjostein NA, editors. *Metal surfaces: structure, energetics and kinetics*. Metals Park, OH: American Society for Metals; 1963. p. 155.
- [27] Blakely JM. *Introduction to the properties of crystal surfaces*. Oxford: Pergamon Press; 1973. p. 261.
- [28] Sutton AP, Balluffi RW. *Interfaces in crystalline materials*. Oxford: Clarendon Press; 1995. p. 819.